Hindawi
International Journal of Polymer Science
Volume 2023, Article ID 6020509, 13 pages
https://doi.org/10.1155/2023/6020509

Research Article

Delamination Characteristics of Aluminum-Composite Bonds: Impact of Reinforcements and Matrices

M. Hussain,[1] A. Imad,[2] A. Saouab,[3] A. Abbas,[1] T. Kanit,[2] S. Shahid,[4] and Y. Nawab[1]

[1]*School of Engineering & Technology, National Textile University, 37610 Faisalabad, Pakistan*
[2]*Univ. Lille, ULR 7512-Unité de Mécanique de Lille Joseph Boussinesq (UML), F-59000 Lille, France*
[3]*Laboratoire Ondes et Milieux Complexes, LOMC, UMR 6294 CNRS, Le Havre University, F–76058 Le Havre, France*
[4]*Department of Biochemistry, Government College Women University Faisalabad, Faisalabad 38040, Pakistan*

Correspondence should be addressed to Y. Nawab; ynawab@ntu.edu.pk

Received 13 September 2023; Revised 2 December 2023; Accepted 12 December 2023; Published 30 December 2023

Academic Editor: Chenggao Li

Adhesion properties of metal-composite bonds are crucial in defining composite capability with other metallic components, and failures could lead to severe accidents. Hence, the study is aimed at the development and characterization of metal-composite bonds using different rigid adherends and adhesive materials (thermoset and thermoplastics). Among natural fibers, jute was used, while aramid, carbon, and glass woven reinforcements were employed from synthetic fibers. A simultaneous comparison of both thermoset and thermoplastic matrices was done using epoxy, polypropylene (PP), and polyvinyl butadiene (PVB) as adhesive materials. Floating roller delamination characterization proved variation in adhesion qualities governing different failure modes by varying adhesive even in a single rigid adherend. The highest fracture toughness was observed for aluminum-jute bonds made with PP and PVB that was due to toughness of matrix and intralaminar failure. Carbon being brittle in nature showed the most fluctuated performance with a 90% difference between the highest value of carbon-PVB and the lowest value of carbon-epoxy. Thermoplastic matrices owing to plasticity offered overall more fracture toughness than brittle thermoset resin. Furthermore, intralaminar was the dominant failure mechanism in the jute-based bond made with thermoplastic matrix.

1. Introduction

Composite materials have gained a significant market value in the automobile and aerospace industries during recent years owing to their lightweight and better mechanical characteristics [1, 2]. Composite materials, being a combination of matrix and reinforcement, could comprise a matrix of thermoset and thermoplastic nature and reinforcements of natural and synthetic origins [3]. Both thermoplastic and thermoset resins offer certain advantages. Similarly, different types of synthetic and natural reinforcements are also used for composite fabrication [4]. However, synthetic reinforcements are being scrutinized due to their environmental issues. Therefore, natural fiber reinforcements are being preferred in this era as a sustainable solution to increasing environmental burdens [5, 6]. As composites are becoming more prevalent in the aerospace, automotive, and transport sectors, therefore, the joining of composite components with metal ones has become increasingly common and tricky at the same time due to variations in the nature of materials [7–9]. Since the alternatives to conventional synthetic reinforcement and thermoset resin are on the rise, therefore, the joining/bonding of these composites is also a new area that requires attention [10].

Different types of metal-composite joining techniques are being used including mechanical, adhesive, and hybrid methods; however, adhesive bonding is the preferred joining technique as it avoids drilling and nut bolting hazards, i.e., stress concentrations, fiber failures, and plies disturbances, etc. [11–15]. Substituting adhesive joints replacing fasteners also helps to speed up the assembly process and cut down on labor costs [16]. However, the interfacial adhesion strength has always remained an area of interest to overcome the interfacial failures of metal composite bonds [17–20].

Table 1: Physical parameters of reinforcements.

Sr. no.	Reinforcement material	Supplier	Areal density (g/m^2)	Thickness (mm)	Plain weave (animated)
1	Jute	Sargodha Jute Mills, Pakistan	220	1.13	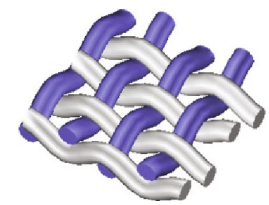
2	Aramid	Yantai Tayho Advanced Materials Co., Ltd, China	220	0.32	
3	Carbon	Formosa Plastics Corporation, Taiwan	200	0.34	
4	Glass	Fibre Craft Industries, Pakistan	231	0.25	

Table 2: Physical and mechanical properties of matrices used for metal-composite bond fabrication.

Sr. no.	Matrix	Supplier/tradename	Tensile strength (MPa)	Tensile modulus (GPa)	Elongation (%)	Glass transition temperature (°C)	Melting temperature (°C)
1	Epoxy	Araldite® LY 556 Aradur® 22962	62-72	2.7-3	3.0-4.0	148-158	—
2	PP	Chawla Industries, Pakistan	30	1.2	115	-10°C	170
3	PVB	Tanyun, China	40-50	2.5	41	66-84	165-200

Various treatments are carried out to enhance the interfacial characteristics. Mechanical treatment is the simplest one where a metal surface is rubbed against sandpaper or any other surface to create a rough surface and active sites for bonding. Similarly, several chemical treatments such as NaOH and anodizing also exist in the market which perform microlevel etching by breaking settled bonds to induce active regions for better adhesions [21]. Metal-composite bond adhesions are assessed using various delamination tests; however, an in vitro destructive test method is widely employed in the interfacial peel-off energy assessment in the aerospace industry termed as floating roller peel-off test [22]. The better the adherend interface bonding, the more energy will be required to peel off, leading towards a better performance [23].

The investigated findings report the metal surface treatments necessary to enhance the adhesion quality through roughening the surface. Among different surface treatment techniques, the anodizing exhibits the highest adhesion for aluminum alloys [24]. Anodized aluminum-lithium alloy-laminated novel fiber-reinforced composites outperform conventional GLARE composites [25]. Hence, anodizing becomes the preferred surface treatment for flexible adherends. Adhesive quantity proves to be influential in determining the adhesion strength of metal-composite bonds. Increasing the adhesive amount enhances the interfacial strength up to an optimum quantity only after which the characteristics decline [26]. Moreover, several compatible adhesives are being developed to increase bonding quality; but still, the generic thermoset and thermoplastic matrices are mostly used [27–29]. Mechanical properties including tensile and impact are influenced by changing stacking sequences in rigid adherends of FMLs, and also by varying the orientation/place of aluminum sheets within FMLs [30, 31]. Similarly, the epoxy-joined FML jute-basalt hybrid sandwich composites consisting of carbon nanotubes exhibit superior flexural and shear performance as compared to unhybrid composites [32]. Changing adherend type affects the peel strength [33]; however, failure modes are also significant to be considered along with applied force during delamination [34]. Failure modes during floating roller testing also vary by ageing, i.e., metal-composite bonds exhibiting cohesive failures shift towards adhesive failure modes after ageing [35].

Though the literature comprises valuable work on the delamination characteristics of metal-composite bonding and much of the emphasis is on thermoset matrix and synthetic fibers, the simultaneous investigation of different thermoset and thermoplastic matrices on different types of natural and synthetic reinforcements is still not investigated. Hence, the research focuses on the development of metal-composite bonds using three different types of thermoset and thermoplastic matrices with four variable fiber woven reinforcements. The delamination characteristics of developed samples were investigated using the floating roller peel test. The mode of failure, fracture toughness, and delaminated surface of tested samples were analyzed to compare the effect of matrix and reinforcement.

2. Materials, Manufacturing, and Testing

Metal-composite bond manufacturing requires a compatible combination, and assembling of rigid adherend, flexible adherend, and adhesive materials. The detailed description of employed materials, manufacturing techniques, and characterization methodology is described in this section.

2.1. Materials Used for the Metal-Composite Bond Manufacturing. The metal-composite bond has three main components, reinforcement, matrix, and metal. Since the

Table 3: Details of samples used in the current study.

Sr. no.	Matrix/adhesive	Reinforcement (rigid adherend)	Metal sheet (flexible adherend)	Specimen code
1	Epoxy			JE
2	PP	Plain woven jute		JP
3	PVB			JB
4	Epoxy			AE
5	PP	Plain woven aramid		AP
6	PVB		Aluminum sheet (0.6 mm)	AB
7	Epoxy			CE
8	PP	Plain woven carbon		CP
9	PVB			CB
10	Epoxy			GE
11	PP	Plain woven glass		GP
12	PVB			GB

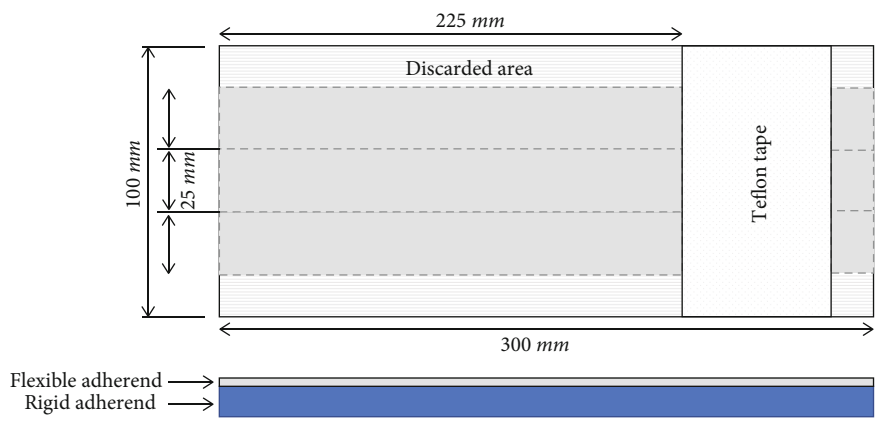

Figure 1: Schematic view of metal composite bond engineering.

floating roller peel test was conducted for the evaluation of adhesion quality, therefore, it has two components: flexible adherend (metal) and rigid adherend (composite). Four different types of woven reinforcement were used in the current study, and details are given in Table 1. The plain weave pattern was followed with simple one-by-one interlacement of warp and weft yarns. Jute woven fabric was used to make natural fiber-based metal-composite bonds. Jute is a natural lignocellulosic fiber that comprises numerous cellulose fibrils and is being widely used in natural fiber-reinforced composites due to its viable mechanical characteristics [36]. Aramid, carbon, and glass woven fabrics were used as synthetic reinforcement as these are used most widely in different types of composite applications.

Along with four types of reinforcements, three different types of matrices were used: thermoset and thermoplastic. Thermoset epoxy of trade name NAN YA NPEF-170 (Taiwan) and hardener Aradur HY 159 were used for thermoset resin-based bonds. Polypropylene (PP) and polyvinylbutyral (PVB) were used as thermoplastic matrices. The above-mentioned matrices were employed in this study viewing their demand in hi-tech application. The physical characteristics of used matrices have been presented in Table 2.

Table 4: Curing parameters of resins.

Sr. no	Resin	Curing time	Temperature
1	Epoxy	40 min	60°C
2	PVB	20 min	155°C
3	PP	10 min	185°C

The 7075-T6 Alclad Aluminum sheet was used as a metal part having a thickness of 0.6 mm.

2.2. Manufacturing Metal-Composite Bond Manufacturing. Since the metal-composite bond involves joining metal and composites with some adhesive materials, hence, the surface of metal needs to be prepared properly for even adhesion. As aluminum was used as a metal in the current study, its surface was anodized using phosphoric acid anodizing. Phosphoric acid anodizing was done following the method used by Hussain et al. [37, 38]. The experimental design comprised two basic factors with three levels; hence, the total number of developed samples was twelve using a full factorial design approach. The design of the experiment is shown in Table 3.

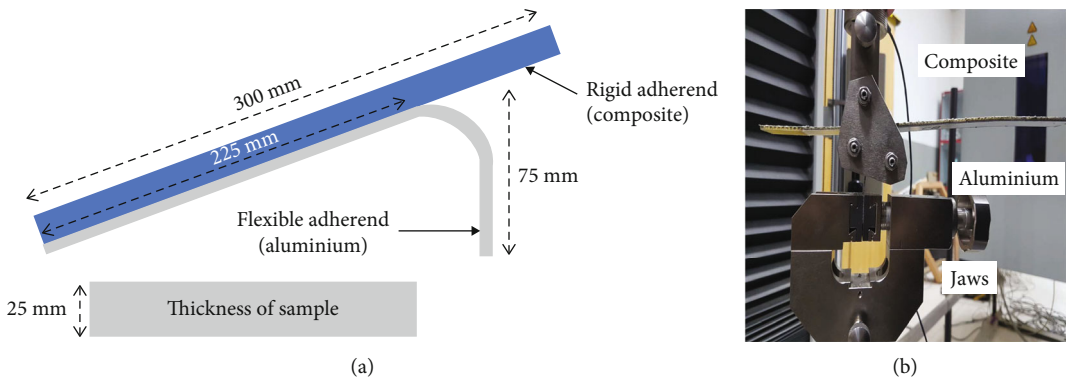

Figure 2: (a) Schematic view of the floating peel roller test. (b) Sample loading on the universal testing machine.

Figure 1 shows the schematics of metal-composite bond manufacturing. A standard discarded area was provided around the flexible adherend attached to the rigid adherend, while the Teflon sheet was employed at the zone where the flexible adherend was to be tilted during the floating roller peel test. After the placement of materials as per Figure 1, the samples were manufactured using standard procedures for respective adhesives. All thermoset samples were prepared by applying the matrix by hand lay-up technique. Epoxy was mixed in a 100 : 12.5 ratio (resin: hardener), before application. After that, the samples were placed in a compression hot press. However, the thermoplastic adhesive comprising specimens was directly manufactured through compression molding. The details of manufacturing temperature and curing time are shown in Table 4.

2.3. Characterization of Metal-Composite Bond. The peel strength of metal-composite adhesive bonds was determined using the DIN EN 2243-2 standard. The test was carried out on a Zwick/Roell UTM Z100 at a testing speed of 152 mm/min. Figure 2(a) shows the schematic of the floating roller peel test specimens, comprised of two adherends termed as rigid and flexible adherends. Similarly, Figure 2(b) shows specimen loading on the universal testing machine. Aluminum was employed as a flexible adhering material, whereas composite (jute, carbon, aramid, and glass) was used as a rigid adherend. The average adhesive layer thickness for epoxy, polypropylene, and polyvinyl chloride was 0.26 ± 0.02 mm, 0.35 ± 0.015 mm, and 0.36 ± 0.016 mm, respectively. All samples have an overall thickness of around 3.2 millimeters. Three tests were performed per specimen for the reproducibility of results.

Using the following Equation (1), the fracture toughness was calculated.

$$\text{Fracture toughness } G = \frac{A}{aw}\left[\frac{J}{m^2}\right], \tag{1}$$

whereas A is the area under the curve, a is the propagated crack length, and w is the width of specimen (25 mm).

3. Results and Discussion

Figure 3(a) depicts the typical force-displacement curve of the floating roller peel test of aluminum-composite bonds. The curve has two zones, the first one is the zone of crack initiation, and the second one is the zone of crack propagation. The crack-initiating zone is the section of the curve at which crack formation begins. Most of the time, the highest force is required in the region to onset the cracks within the matrix. The second zone corresponds to the crack propagation phase since the fracture propagates with some variability in the curve in this region. The behavior of the curve in this zone depicts the effect of matrix, reinforcement, and bonding quality. This zone shows the type of failure, i.e., cohesive, adhesive, or intralaminar, etc. Three tests were carried out for each specimen for repeatability of results as shown in Figure 3(b) (jute and PVB laminate), from which the averaged curve was considered for final analysis.

Figure 4 highlights four different failure modes of aluminum-composite bonds observed in the current study, and these failure modes give the characteristics of failure modes of bonds made with different type of reinforcement and matrix. The cohesive failure is observed when the only matrix layer is cracked, and the crack propagates solely in matrix layer. The cohesive failure is the desired type of failure as the bond does not fail at one of interface points. In adhesive failure, the failure occurs at one of the interfaces either between metal-matrix or composite-matrix. This type of failure shows the weakest bonding. In mix mode failure, both cohesive and adhesive failures occur simultaneously. However, in intralaminar failure, some of the fiber portion from composite is peeled off and remains sticked with matrix on flexible adherend [39, 40]. Even cohesive failure is desired in the metal-composite bonds; however, in the current study, the intralaminar failure gives the highest delamination force and was most dominant for thermoplastic-based bonds. The plasticity of the flexible adherend material and adhesive layer also adds to the delamination performance during the floating roller test. Due to the fact that in the present investigation, just the adhesive material type is altered for each sample set and the ductility of the adhesive material contributed considerably to the final parameters.

3.1. Aluminum-Jute Composite Bond. The force-displacement curves of epoxy, PP, and PVB-bonded aluminum-jute

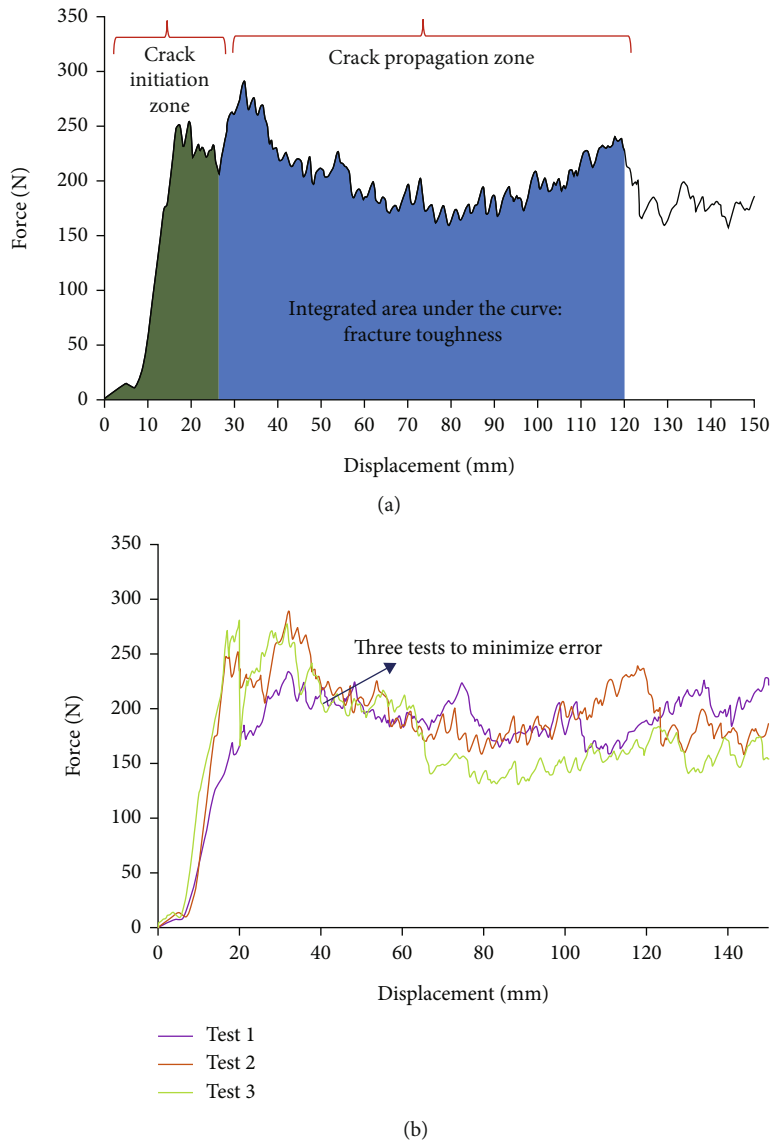

Figure 3: (a) The typical force-displacement curve of t-peel tests of metal-composite bond. (b) Force-displacement curves of three t-peel tests.

composites have been shown in Figure 5. All the curves exhibited significantly distinct delamination behaviors, indicating that the aluminum-jute composite bonds have variable delamination characteristics due to different behavior of matrix. As the JE demonstrates, the curve has a sharp peak. The brittle epoxy matrix yields these numerous sharp peaks. In the crack propagation zone of thermoplastic matrix-based bonds, there are varying zones, as seen by the varying slopes of the JP and JB curves. These different peaks show the type of failure that occurred during delamination; the higher force relates to intralaminar fiber failure which results in high delamination force that can be seen in Figures 6(a) and 6(b). The JB sample exhibits the higher delamination force when compared to JP that is mainly related to higher plastic deformation, intralaminar failure, and strong bonding nature of PVB [41, 42].

Different force-displacement behaviors governed different fracture modes in aluminum-composite bonds. Figure 6 shows the delaminated surfaces of tested specimens. The surface of JE's aluminum was glutted with epoxy; however, JP and JB contain spots of adhered resin on both metal and composite surfaces. Intralaminar fiber failure can be seen on the delaminated surfaces of both the PP and PVB composites. For JP and JB, the fibers are visible on the adhesive on aluminum surface. The delamination behavior is also inferred from the flexible adherend conformation after characterization. The slanted PVB-aluminum sample in Figure 6(c) represents that PVB-based bonds offer the highest resistance, followed by the JP and JE aluminum bonds. Such delamination behaviors indicate that PVB adhesive bond is tougher than epoxy and PP adhesive bonds and involves multiple failure phenomena. Interfacial failures between adhesive, aluminum, and composite are also vital in delamination behaviors. The adhesive layer's interaction with the aluminum in JE adhesive aluminum bond was apparently strong due to bonding between epoxy and aluminum. Unlike epoxy, the PP in jute-PP composites forms mechanical bridging; therefore, failure in the

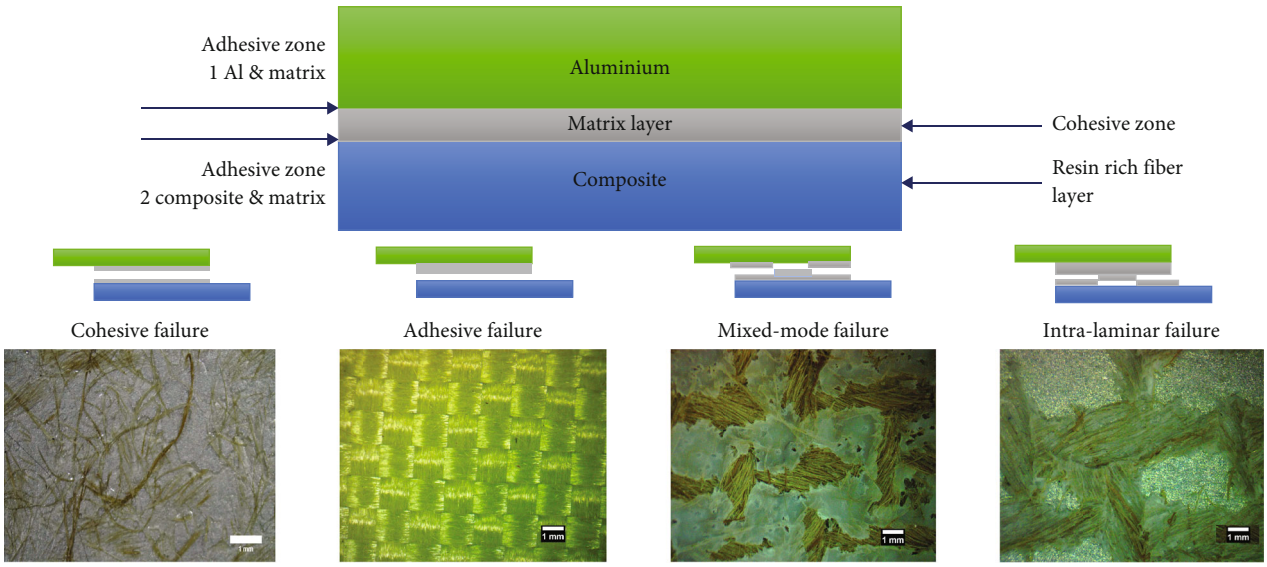

Figure 4: Variable failure modes of metal composite bonds.

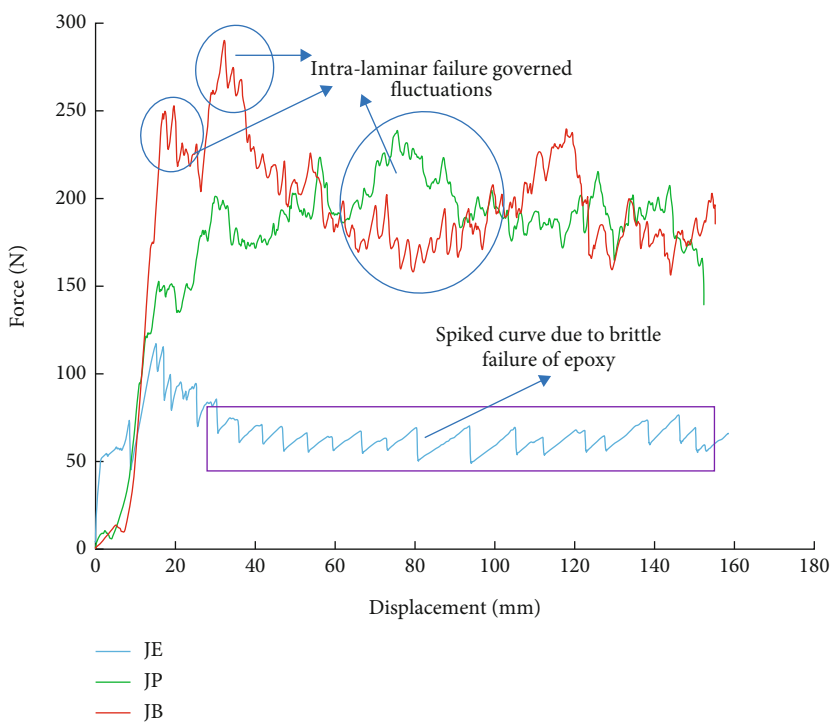

Figure 5: Force-displacement curves of aluminum-jute composite bond.

material occurs in both composite and aluminum interface. An intriguing example is the jute-PVB aluminum adhesive bond, which has significantly greater adhesive failure but more debonding force. The adhesive disintegration was particularly severe towards the aluminum surface. Such trend was due to significant ductility, and the fact that with aluminum only, a small adhesive layer at interface, which provokes the failure at aluminum interface, further the jute-PVB composite was stronger to witness delamination on composite surface.

3.2. Aluminum-Aramid Composite Bond. Force-displacement curves for the floating roller peel test of aluminum-aramid composite bonds have been shown in Figure 7. A closer look at the curve reveals that the AP exerts the most delamination force, followed by the AB and the AE aluminum bonds. Polypropylene matrix possesses a viable strength-to-weight ratio and is widely used in thermoplastic composites. Properties of PP and PVB are comparable; however, the trends could deviate depending on the type of

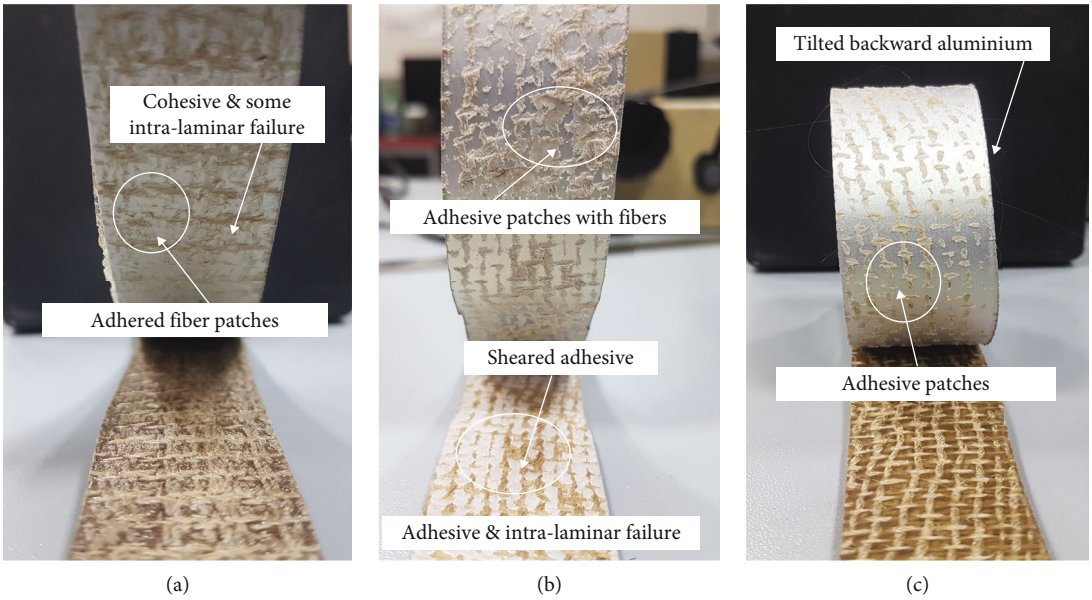

Figure 6: Delaminated surfaces: (a) Jute-epoxy, (b) Jute-PP, and (c) Jute-PVB.

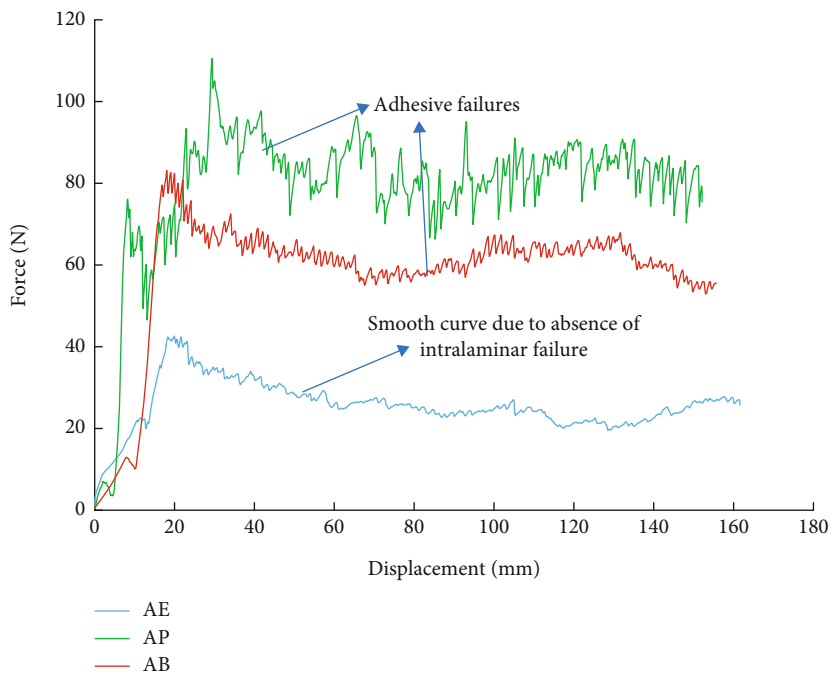

Figure 7: Force-displacement curves of aluminum-aramid composite bonds.

reinforcing material and processing conditions [43]. A Higher force for PP can be related to the described fact. Slight bumps appear on the AE curve due to brittle behaviour of epoxy. Delamination is smooth in the crack propagation region, and the fibers did not stick to the matrix as the crack propagated. Additionally, the AB demonstrates that the crack spread without any hiccups after its primary initiation. However, the AP showed considerable curve unevenness at the crack initiation and propagation zones, indicating that PP matrix cracking was not homogeneous. Regardless of the type of reinforcement and matrix, the failure was adhesive, which was due to properties of aramid which renders fiber pullout.

It can be seen in Figure 8 that the matrix solely adhered with flexible adherend aluminum, and there was no evidence of fiber pull-out on the delaminated interfaces for all adhesive types. Apparently as can be determined, the intrinsic properties of the aramid fibers used in the composite had prevented intralaminar failure from occurring. Furthermore, the adhesive layer attached to the aluminum displays the characteristic fingerprint of a plain weave pattern. This reveals that the interface between the flexible adherend

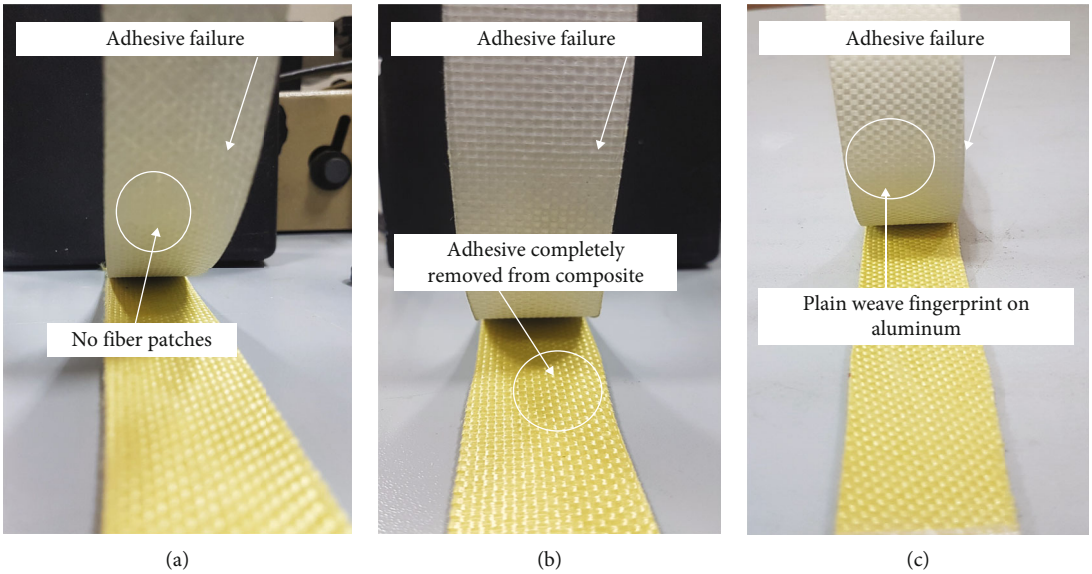

Figure 8: Delaminated surfaces: (a) aramid-epoxy, (b) aramid-PP, and (c) aramid-PVB.

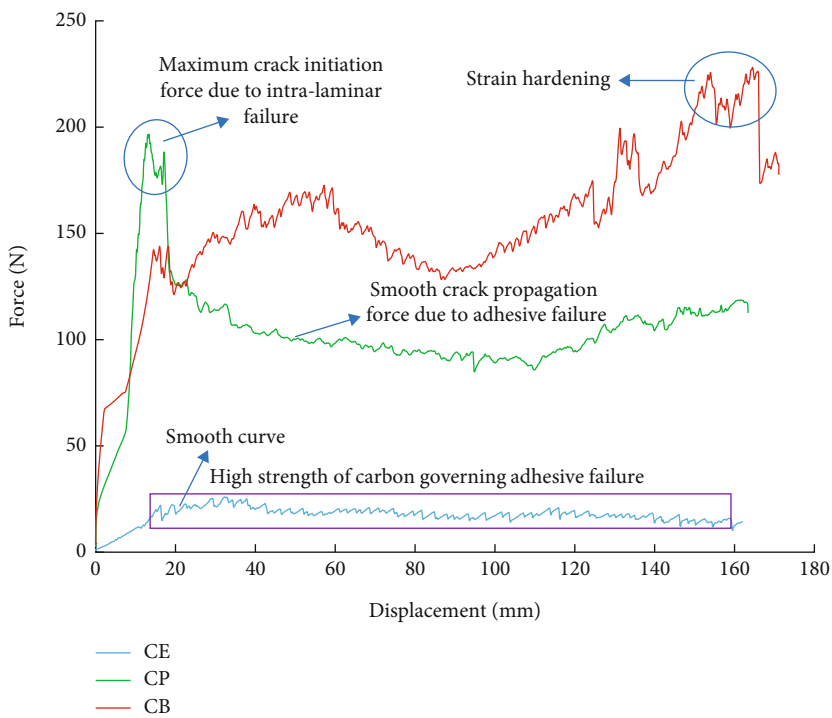

Figure 9: Force-displacement curves of aluminum-carbon composite bonds.

aluminum and matrix was significant, and the bond failed primarily due to adhesive failure. The differential ductility of adhesives and fiber matrix interfaces accounted for the variation in force, even though the failure modes were similar.

3.3. Aluminum-Carbon Composite Bond. Figure 9 displays the force-displacement behaviors of characterized aluminum-carbon composite bond specimens using different adhesives. Once the fracture has begun, the CE travels along a remarkably smooth trajectory. Mainly, it demonstrates uniform crack initiation and propagation. In contrast to the CB, the CP has a markedly different behavior, with an initially strong crack initiation force accompanied by a drop in force for fracture progression region. Within the cracking propagation zone, the force exerted on the CB continues rising; however, its form and rate of increase are not constant. The curves of CP and CB show different patches, that patches occur due to delamination behavior, and the highest peak was observed due to intralaminar fiber failure. This can also be seen in the delaminated samples.

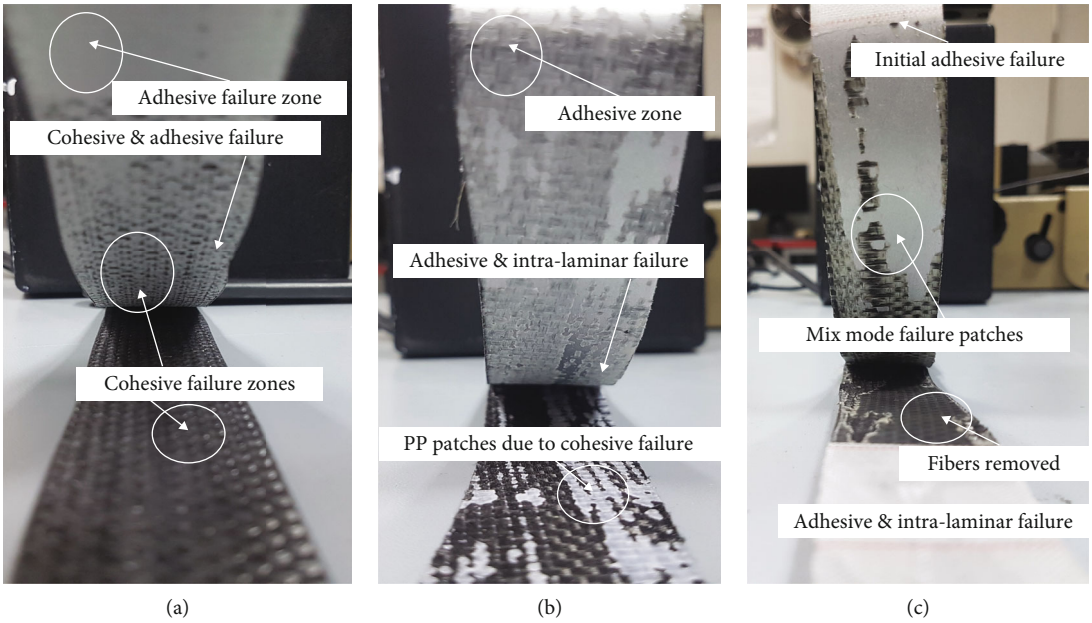

Figure 10: Delaminated surfaces: (a) carbon-epoxy, (b) carbon-PP, and (c) carbon-PVB.

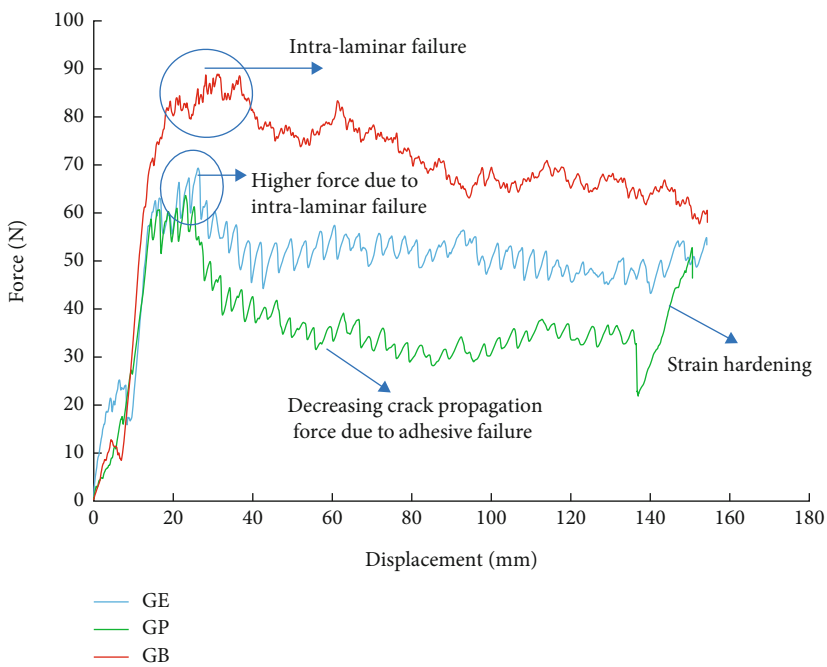

Figure 11: Force-displacement curves of aluminum-glass composite bonds.

Figure 10 highlights the deboned surfaces of CE, CP, and CE specimens. Debonding of CE surfaces reveals matrix adhesion to both composite and aluminum. Certain carbon fibers that had been adhered with matrix exhibited slight intralaminar failure, although the primary failure mode was cohesive. Adhesive failure and intralaminar failures have been seen in the CP. Both the carbon fibers and the adhesive layer could be spotted on the adhered patches of intralaminar failure. Adhesive failure for the CB occurred along with intralaminar failure mode. Adhesive failure occurred first at the metal-matrix interface before transitioning to intralaminar failure later on. In the same way, the CB curve's peculiarities could be traced back to this failure mode. CB incorporates both intralaminar and adhesive failure modes. The failure process of aluminum-carbon composite bonds reveals that, despite more dominating cohesive failures in CE, the debonding force was greater for PP and PVB adhesive metal bonds. Thermoplastic matrix's ductile nature was mainly responsible for this along with intralaminar failure. Since there is also failure involved in composite layer

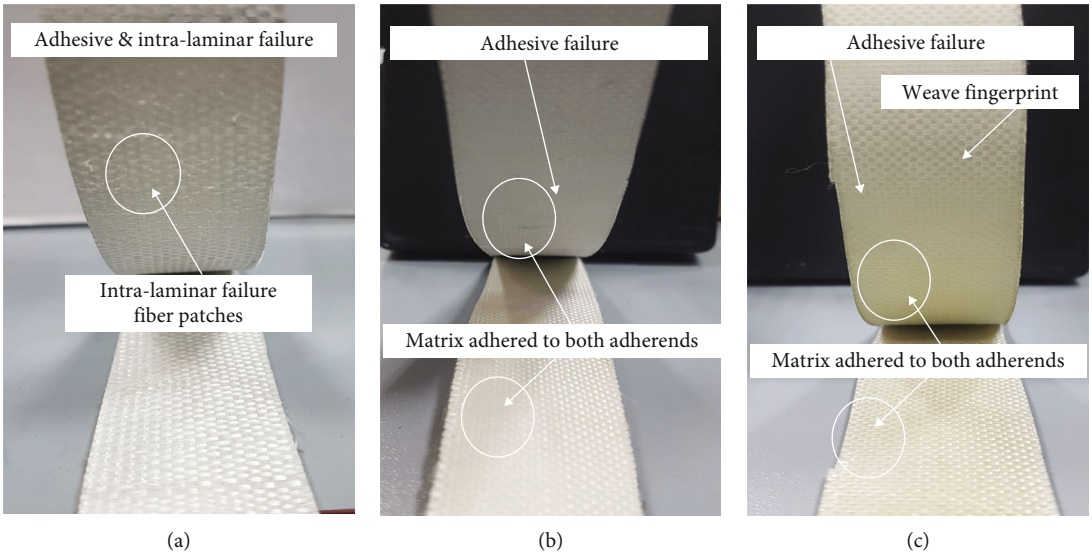

Figure 12: Delaminated surfaces: (a) glass-epoxy, (b) glass-PP, and (c) glass-PVB.

Table 5: Average delamination force and failure modes of metal-composite bonds.

Sr#	Sample type	Average delamination force	Type of failure
1.	JE	61.8 ± 3.61	Cohesive & intralaminar
2.	JP	191.5 ± 3.90	Adhesive & intralaminar
3.	JB	188.3 ± 8.49	Adhesive & intralaminar
4.	AE	20.38 ± 5.07	Adhesive
5.	AP	68.3 ± 4.02	Adhesive
6.	AB	78 ± 6.12	Adhesive
7.	CE	15.69 ± 2.15	Mix-mode failure
8.	CP	107.6 ± 9.39	Adhesive & intralaminar
9.	CB	173.7 ± 16.17	Adhesive & intralaminar
10.	GE	35.4 ± 5.32	Adhesive & intralaminar
11.	GP	52.2 ± 4.43	Adhesive
12.	GB	66.1 ± 6.36	Adhesive

during intralaminar failure, hence, it is a favorable one than adhesive failure.

3.4. Aluminum-Glass Composite Bond. Among glass-reinforced metal-composite bonds with different adhesives, the glass-epoxy (GE) bond shows the highest fracture initiating and propagating forces (Figure 11). The crack propagation region of GB was smoothly declining, but in GP, it fluctuated. Delaminated surfaces of GE entailed in Figure 12 reveal both fibers and adhesive adhered on flexible adherend due to intralaminar failure. For polypropylene, there was no evidence of intralaminar fiber failure on the composite facade, while the flexible adherend was covered with PP. Most failures occurred at the composite/matrix interface, where adhesive failure predominated. The GB also displays the PVB matrix completely covering the flexible adherend. Adhesive failure was the primary failure mode, while there were also some intralaminar failures. Fiber failure in the composite portions of both GE and GB metal bonds can be observed. Matrix adhesion to the aluminum surface is clearly visible on both GB and GE. Although the GP's matrix was bonded to the aluminum's surface, the composite component showed no signs of fiber pull-out.

3.5. Performance Evaluation

3.5.1. Comparison of Delamination Force and Type of Failure. Table 5 highlights the average delamination force born by different metal-composite bonds w.r.t type of failure occurred. Epoxy being brittle exhibited the least average delamination forces than other adhesives used, for all jute, aramid, carbon, and glass reinforcements. Mix mode and intralaminar failures experiencing metal-composite bonds had higher delamination forces than cohesive failures. Adhesive failure average delamination forces are almost equivalent to intralaminar failures.

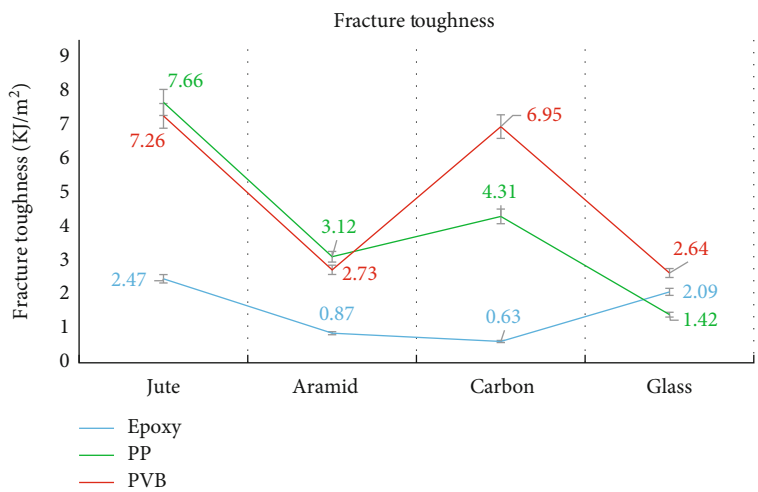

Figure 13: Fracture toughness of metal-composite bonds.

3.5.2. Fracture Toughness. All the samples' fracture toughness was determined using the aforementioned criteria in Equation (1). Comparison of fracture toughness provides insight into the overall characteristics of the material and the influence of the failure modes. The fracture toughness of metal-composite bonds engineered with various fibers and matrices is compared graphically in Figure 13. Overall, the data demonstrate that thermoplastic adhesives outperform epoxy in terms of fracture toughness. The intralaminar failures of jute and carbon resulted in a high fracture toughness. Overall, aramid and glass' poor fracture toughness could be attributed to significant adhesive failures. With a large proportion of intralaminar failure and low modulus yarn, epoxy exhibited the highest fracture toughness for glass and jute yarns. The PVB demonstrated its efficacy with all types of reinforcements when the overall fracture toughness was compared w.r.t matrix and reinforcement types.

4. Conclusion

Adhesion characteristics were evaluated using the floating roller peel test. The characterization proved to be influential in determining the failure modes of different thermosets and thermoplastic adhesives with variable rigid adherends and aluminum. Thermoplastic adhesives had more energy absorption in terms of fracture toughness than thermoset ones due to the brittle nature of epoxy and plastic nature of the thermoplastic matrix. A significant difference was observed for jute reinforcement, where PP and PVB exhibited 210% and 194% higher fracture toughness than epoxy-jute composite metal bonds. Jute-reinforced rigid adherends comprising metal-composite bonds exhibited intralaminar failure modes, making jute a suitable rigid adherend preventing adhesive and cohesive failures like aramid, carbon, and glass, respectively. Such cohesive failure made the fracture toughness trend different for glass reinforcement, i.e., PP had about 32% less fracture toughness than epoxy, though the PVB still exhibited 26% higher fracture toughness than epoxy. Some of the carbon-aluminum bonds exhibited minor intralaminar failures. Metal composite bonds with jute and aramid possessed the highest fracture toughness values for PP, while the PVB showed the higher fracture toughness with jute and carbon-reinforced rigid adherends. However, for jute-reinforced rigid adherend, PP has 5.5% better performace than PVB, exhibiting an overall highest fracture toughness.

Data Availability

Data will be made available on request.

Conflicts of Interest

The authors declare that they have no known competing financial interests or personal relationships that could have appeared to influence the work reported in this paper.

Acknowledgments

The authors would like to thank the National Centre for Composites Materials NCCM, National Textile University, Pakistan, for helping in the fabrication and testing of metal-composite joints.

References

[1] A. Arablouei and V. Kodur, "Cohesive zone model properties for evaluating delamination of spray-applied fire-resistive materials from steel structures," *Engineering Fracture Mechanics*, vol. 143, pp. 138–157, 2015.

[2] S. T. de Freitas and J. Sinke, "Test method to assess interface adhesion in composite bonding," *Applied Adhesion Science*, vol. 3, no. 1, 2015.

[3] A. Ali, K. Shaker, Y. Nawab et al., "Hydrophobic treatment of natural fibers and their composites—a review," *Journal of Industrial Textiles*, vol. 47, no. 8, pp. 2153–2183, 2018.

[4] H. Awais, Y. Nawab, A. Amjad, A. Anjang, H. Md Akil, and M. S. Zainol Abidin, "Environmental benign natural fibre reinforced thermoplastic composites: a review," *Composites Part C: Open Access*, vol. 4, 2021.

[5] K. Shaker, M. Ashraf, M. Jabbar et al., "Bioactive woven flax-based composites: development and characterisation," *Journal of Industrial Textiles*, vol. 46, no. 2, pp. 549–561, 2016.

[6] M. M. Rehman, M. Zeeshan, K. Shaker, and Y. Nawab, "Effect of micro-crystalline cellulose particles on mechanical properties of alkaline treated jute fabric reinforced green epoxy composite," *Cellulose*, vol. 26, no. 17, pp. 9057–9069, 2019.

[7] S. Abrate, J. F. Ferrero, and P. Navarro, "Cohesive zone models and impact damage predictions for composite structures," *Meccanica*, vol. 50, no. 10, pp. 2587–2620, 2015.

[8] S. Jiang, J. Ma, Z. Liu, and H. Guo, "Scientometric analysis of artificial intelligence (AI) for geohazard research," *Sensors*, vol. 22, no. 20, p. 7814, 2022.

[9] J. Ma, D. Xia, Y. Wang et al., "A comprehensive comparison among metaheuristics (MHs) for geohazard modeling using machine learning: insights from a case study of landslide displacement prediction," *Engineering Applications of Artificial Intelligence*, vol. 114, article 105150, 2022.

[10] Y. Yamagata, X. Lu, Y. Sekiguchi, and C. Sato, "Experimental investigation of mode i fracture energy of adhesively bonded joints under impact loading conditions," *Applied Adhesion Science*, vol. 5, no. 1, 2017.

[11] H. Aghamohammadi, S. N. Hosseini Abbandanak, R. Eslami-Farsani, and S. M. H. Siadati, "Effects of various aluminum surface treatments on the basalt fiber metal laminates interlaminar adhesion," *International Journal of Adhesion and Adhesives*, vol. 84, pp. 184–193, 2018.

[12] G. Jeevi, S. K. Nayak, and M. Abdul Kader, "Review on adhesive joints and their application in hybrid composite structures," *Journal of Adhesion Science and Technology*, vol. 33, no. 14, pp. 1497–1520, 2019.

[13] A. Galińska and C. Galiński, "Mechanical joining of fibre reinforced polymer composites to metals—a review. Part II: riveting, clinching, non-adhesive form-locked joints, pin and loop joining," *Polymers*, vol. 12, no. 8, p. 1681, 2020.

[14] A. Pramanik, A. K. Basak, Y. Dong et al., "Joining of carbon fibre reinforced polymer (CFRP) composites and aluminium alloys – a review," *Composites. Part A, Applied Science and Manufacturing*, vol. 101, pp. 1–29, 2017.

[15] S. D. Thoppul, J. Finegan, and R. F. Gibson, "Mechanics of mechanically fastened joints in polymer-matrix composite structures - a review," *Composites Science and Technology*, vol. 69, no. 3–4, pp. 301–329, 2009.

[16] S. Deng, L. Djukic, R. Paton, and L. Ye, "Thermoplastic–epoxy interactions and their potential applications in joining composite structures – a review," *Composites. Part A, Applied Science and Manufacturing*, vol. 68, pp. 121–132, 2015.

[17] X. Zhou, Y. Zhao, X. Chen, Z. Liu, J. Li, and Y. Fan, "Fabrication and mechanical properties of novel CFRP/Mg alloy hybrid laminates with enhanced interface adhesion," *Materials and Design*, vol. 197, article 109251, 2021.

[18] L. Hamill and S. Nutt, "Adhesion of metallic glass and epoxy in composite-metal bonding," *Composites Part B: Engineering*, vol. 134, pp. 186–192, 2018.

[19] J. M. Arenas, C. Alía, J. J. Narbón, R. Ocaña, and C. González, "Considerations for the industrial application of structural adhesive joints in the aluminium–composite material bonding," *Composites Part B: Engineering*, vol. 44, no. 1, pp. 417–423, 2013.

[20] H. Y. Yang, Z. Wang, L. Y. Chen, S. L. Shu, F. Qiu, and L. C. Zhang, "Interface formation and bonding control in high-volume-fraction (TiC+TiB2)/Al composites and their roles in enhancing properties," *Composites Part B: Engineering*, vol. 209, article 108605, 2021.

[21] Y. Hu, B. Yuan, F. Cheng, and X. Hu, "NaOH etching and resin pre-coating treatments for stronger adhesive bonding between CFRP and aluminium alloy," *Composites Part B: Engineering*, vol. 178, article 107478, 2019.

[22] M. Y. Khalid, A. Al Rashid, and M. F. Sheikh, "Effect of anodizing process on inter laminar shear strength of GLARE composite through T-peel test: experimental and numerical approach," *Experimental Techniques*, vol. 45, no. 2, pp. 227–235, 2021.

[23] S. M. R. Khalili, M. Sharafi, R. Eslami-Farsani, and A. Saeedi, "Effect of thermal cycling on tensile properties of degraded FML to metal hybrid joints exposed to sea water," *International Journal of Adhesion and Adhesives*, vol. 79, pp. 95–101, 2017.

[24] X. Zheng, Z. Zhao, Z. Chu, H. Yin, and W. Wang, "Effect of surface treatment methods on the interfacial behavior of fiber metal laminate based on WE43 magnesium alloy," *International Journal of Adhesion and Adhesives*, vol. 110, p. 102957, 2021.

[25] H. Li, Y. Hu, Y. Xu et al., "Reinforcement effects of aluminum–lithium alloy on the mechanical properties of novel fiber metal laminate," *Composites Part B: Engineering*, vol. 82, pp. 72–77, 2015.

[26] H. Li, Y. Hu, X. Fu, X. Zheng, H. Liu, and J. Tao, "Effect of adhesive quantity on failure behavior and mechanical properties of fiber metal laminates based on the aluminum–lithium alloy," *Composite Structures*, vol. 152, pp. 687–692, 2016.

[27] G. Lawcock, L. Ye, Y. W. Mai, and C. T. Sun, "The effect of adhesive bonding between aluminum and composite prepreg on the mechanical properties of carbon-fiber-reinforced metal laminates," *Composites Science and Technology*, vol. 57, no. 1, pp. 35–45, 1997.

[28] A. Nasreen, K. Shaker, and Y. Nawab, "Effect of surface treatments on metal–composite adhesive bonding for high-performance structures: an overview," *Composite Interfaces*, vol. 28, no. 12, pp. 1221–1256, 2021.

[29] R. A. Pethrick, "Design and ageing of adhesives for structural adhesive bonding – a review," *Proceedings of the Institution of Mechanical Engineers, Part L: Journal of Materials: Design and Applications*, vol. 229, no. 5, pp. 349–379, 2015.

[30] S. Mirzamohammadi, R. Eslami-Farsani, and H. Ebrahimnezhad-Khaljiri, "The experimental assessment of carbon nanotubes incorporation on the tensile and impact properties of fiber metal laminate fabricated by jute/basalt fabrics-aluminum layers: as hybrid structures," *Proceedings of the Institution of Mechanical Engineers, Part C: Journal of Mechanical Engineering Science*, vol. 237, no. 8, pp. 1877–1886, 2023.

[31] S. Mirzamohammadi, R. Eslami-Farsani, and H. Ebrahimnezhad-Khaljiri, "The effect of hybridizing natural fibers and adding montmorillonite nanoparticles on the impact and bending properties of eco-friendly metal/composite laminates," *Advanced Engineering Materials*, vol. 25, no. 12, 2023.

[32] S. Mirzamohammadi, R. Eslami-Farsani, and H. Ebrahimnezhad-Khaljiri, "The characterization of the flexural and shear performances of laminated aluminum/jute–basalt fibers epoxy composites containing carbon nanotubes: as multi-scale hybrid structures," *Thin-Walled Structures*, vol. 179, article 109690, 2022.

[33] J. P. O. Pereira, R. G. S. G. Campilho, P. J. R. O. Nóvoa, F. J. G. Silva, and D. C. Gonçalves, "Adherend effect on the peel

strength of a brittle adhesive," in *Procedia Structural Integrity*, pp. 722–729, Elsevier B.V., 2021.

[34] S. T. de Freitas and J. Sinke, "Adhesion properties of bonded composite-to-aluminium joints using peel tests," *The Journal of Adhesion*, vol. 90, no. 5–6, pp. 511–525, 2014.

[35] S. Teixeira de Freitas, M. D. Banea, S. Budhe, and S. de Barros, "Interface adhesion assessment of composite-to-metal bonded joints under salt spray conditions using peel tests," *Composite Structures*, vol. 164, pp. 68–75, 2017.

[36] A. Roy, B. Adhikari, and S. B. Majumder, "Equilibrium, kinetic, and thermodynamic studies of azo dye adsorption from aqueous solution by chemically modified lignocellulosic jute fiber," *Industrial and Engineering Chemistry Research*, vol. 52, no. 19, pp. 6502–6512, 2013.

[37] M. Hussain, A. Imad, Y. Nawab, A. Saouab, C. Herbelot, and T. Kanit, "Effect of matrix and hybrid reinforcement on fibre metal laminates under low–velocity impact loading," *Composite Structures*, vol. 288, article 115371, 2022.

[38] M. Hussain, A. Imad, A. Saouab et al., "Properties and characterization of novel 3D jute reinforced natural fibre aluminium laminates," *Journal of Composite Materials*, vol. 55, no. 14, pp. 1879–1891, 2021.

[39] S. Teixeira de Freitas and J. Sinke, "Failure analysis of adhesively-bonded skin-to-stiffener joints: metal–metal vs. composite–metal," *Engineering Failure Analysis*, vol. 56, pp. 2–13, 2015.

[40] N. Zimmermann and P. H. Wang, "A review of failure modes and fracture analysis of aircraft composite materials," *Engineering Failure Analysis*, vol. 115, article 104692, 2020.

[41] S. Chen, X. Chen, and X. Wu, "The mechanical behaviour of polyvinyl butyral at intermediate strain rates and different temperatures," *Construction and Building Materials*, vol. 182, pp. 66–79, 2018.

[42] A. K. Dhaliwal and J. N. Hay, "The characterization of polyvinyl butyral by thermal analysis," *Thermochimica Acta*, vol. 391, no. 1–2, pp. 245–255, 2002.

[43] P. Yeole, H. Ning, and A. A. Hassen, "Development and characterization of a polypropylene matrix composite and aluminum hybrid material," *Journal of Thermoplastic Composite Materials*, vol. 34, no. 3, pp. 364–381, 2021.